Proceedings of the International Association for Shell and Spatial Structures (IASS) Symposium 2009, Valencia
Evolution and Trends in Design, Analysis and Construction of Shell and Spatial Structures
28 September – 2 October 2009, Universidad Politecnica de Valencia, Spain
Alberto DOMINGO and Carlos LAZARO (eds.)

Modeling sliding cables and geodesic lines through dynamic relaxation

Ruy M.O. PAULETTI*, Daniel M. GUIRARDI, Samir GOUVEIA

* Department of Structural and Geotechnical Engineering
Polytechnic School of the University of São Paulo
Av. Prof. Almeida Prado, trav. 2, n. 8, 05508-900, São Paulo – SP, Brazil.
pauletti@usp.br

Abstract

The Dynamic Relaxation Method (DRM) is an interesting alternative to solve complicated nonlinear equilibrium problems, solved via a pseudo-dynamic analysis, with explicit time integration, carried out exclusively by fast vector manipulations. In the current paper, we present the theoretical formulation and the implementation of the load vectors of a class of finite elements capable of representing the slippage between border cables and membrane sheaths, without friction. The paper also details some improvements in a procedure to search geodesic lines onto triangle-faceted surfaces, relating the expression of the internal load vector of the geodesic string element to the internal vector of a sliding-cable super-element, and proposing a new average nodal normal vector, insensitive to the arbitrary division of a given geometry into different triangular meshes.

Keywords: dynamic relaxation, geodesic-string super-element, sliding-cable super-element.

1. Introduction

Slippage between border cables and membrane sheaths is usually disregarded in finite element analysis of membrane structures, since these cables are commonly represented by a sequence of no-compression truss elements, connected to the membrane elements by their end nodes. In this way any possible sliding between cables and membrane is overruled. Some preliminary numerical investigations suggest, however, that disregarding the slippage between border cables and membrane sheaths may lead to underestimation of membrane stresses, close to the membrane vertices, as well as concealing regions were the membrane goes slack, under the action of wind loads.

A general problem of sliding between cable and membrane would be provided, for instance, by a stabilizing cable sliding over a membrane surface in a generic way, creasing the membrane as it moved, perhaps even locally loosing contact, when the membrane surface becomes concave. In this paper, however, we restrict ourselves to study the cases where the

cable is transversally constrained by the membrane surface, in such a way that sliding is only possible tangentially to the cable development. This is the case of the cables commonly used along the border of the membranes, as well as of internal ridge or valley cables. We will refer to all of these cables, generically, as "border cables".

For small to medium size structures, when the cable diameters are small and the fabrics more flexible, a practical solution to transfer the transversal loads from the membrane to the border cables is the use of sheaths, welded or sewn directly to the membrane fabric. For larger spans, such as in Denver's Airport, less flexible fiberglass fabrics and larger cable diameters are required, so the border cable is positioned externally to the membrane, and a more complicated detailing is required to guarantee slippage and avoid stress concentrations, as described in [1].

Even thou Newton's method usually yields the fastest algorithm for the solution of nonlinear static equilibrium of cable and membrane structures, the dynamic relaxation method may be an interesting alternative to solve complicated nonlinear equilibrium problems, especially when derivatives of the force vectors are not available. The DR Method also provides a tool for the heuristic validation of the more exacting implementations of Newton's Method. Thus, results obtained in the current paper are used to validate those obtained for the same models, but solved via Newton´s Method, as also described in [1].

1.1. Dynamic Relaxation

In the DR method, the problem of the static equilibrium is solved *via* a dynamic analysis, with explicit time integration, and fictitious diagonal mass and damping matrices, arbitrarily chosen to control the stability of the time integration process, according to

$$m_i \ddot{\mathbf{u}}_i + c_i \dot{\mathbf{u}}_i + \mathbf{p}_i\left(\mathbf{u}_j\right) = \mathbf{f}_i \,, \quad i, j = 1, \ldots, n \tag{1}$$

where $m_i, c_i, \mathbf{u}_i, \mathbf{p}_i\left(\mathbf{u}_j\right), \mathbf{f}_i$, are respectively the mass, the viscous damping, displacements, internal and external nodal forces of the i^{th} (or j^{th}) node of the (already discretized) structure. This pseudo-dynamic system can be solved exclusively by vector manipulations, which render very fast the calculation of every time-step. However, precision is usually obtained after a large number of time increments, since explicit time integration is only conditionally stable. Pauletti [2] refers to some pioneering and recent literature on the dynamic relaxation method, pointing out that although the dynamic relaxation method shows no advantage for small to medium sized typical membrane problems, compared to Newton's Method, there may be economy for very large problems.

The system of n nodal equations given by (1) can be grouped in a single matrix equation, according to

$$\mathbf{M}\ddot{\mathbf{u}} + \mathbf{C}\dot{\mathbf{u}} + \mathbf{P}\left(\mathbf{u}\right) = \mathbf{F} \tag{2}$$

where $\mathbf{M}$ and $\mathbf{C}$ are diagonal matrices which collect the nodal masses and viscous dampers, and $\mathbf{P}$ and $\mathbf{F}$ are respectively the *global internal and external force vectors*, which collect the forces acting on every node of the structure. Instead of using a viscous

damping matrix, however, we consider the process of *kinetic damping* [3], with the undamped ($\mathbf{C} = \mathbf{0}$) movement of the structure being followed until a maximum of the total kinetic energy of the system is observed, and all the velocity components of the structure are cancelled, keeping the current geometry. The dynamic analysis is then restarted until new kinetic energy maxima (usually smaller than the precedent ones) are found, and all velocities are zeroed again. The process is repeated until all kinetic energy is dissipated, thus reaching a static equilibrium configuration. The transient of the system's kinetic energy provides a visual criterion for convergence.

Load contributions from every element are added to the global internal force vector according to

$$\mathbf{P} = \sum_{e=1}^{nel} \mathbf{A}^{eT} \mathbf{p}^{e} \tag{3}$$

where $\mathbf{A}^{e}$ is a convenient *Boolean incidence matrix* of the e^{th} element, which relates the element's local degrees of freedom to the global ones. Of course, it is not convenient to perform the matrix multiplications presented in (3), being quite more economical to add the element contributions directly to the global stiffness matrix, as explained in standard FEM textbooks.

2. Internal load vector for a cable element

Consider that cables are approximated by an assemblage of truss elements. Figure 1 depicts a generic, e^{th} element in a current configuration, with nodes indexed as *i* and *j*, in the global structural system, and as *1* and *2*, in the element numeration system.

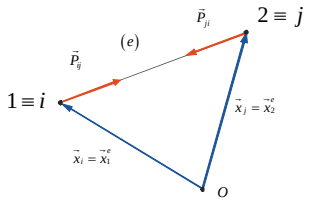

Figure 1: A truss element, with local and global nodal indexes.

Keeping implicit the element index *e*, for basic quantities, we define the vector $\mathbf{l} = \mathbf{x}_2 - \mathbf{x}_1$, and the current element length is given by $\ell = \|\mathbf{l}\|$, whilst $\mathbf{v} = \mathbf{l} / \ell$ is the unit vector directed form node *1* to node *2*, the element is described in an initial configuration, already under a normal force N^0. Thus the reference, zero-stress element length, is given by $\ell^r = EA\ell^0 / \left(EA + N^0\right)$ and the normal force acting on the element, at each instant, is given by $N = EA\left(\ell - \ell^r\right) / \ell^r$, if $\ell > \ell^r$, or $N = 0$, $\ell \le \ell^r$, since a cable cannot withstand compression.

The *internal forces vector* for a truss element is given by

$$\mathbf{p}^e = \begin{bmatrix} -\mathbf{v} \\ \mathbf{v} \end{bmatrix} N \tag{4}$$

The contribution of a generic element defined by nodes $\{i, j\}$ to the global internal load vector is given by (3), with $\mathbf{A}^e_{1i} = \mathbf{A}^e_{2j} = \mathbf{I}_3$ and $\mathbf{A}^e_{1m} = \mathbf{A}^e_{2m} = \mathbf{O}$, $m \in \{1,2,\ldots n_n\} \setminus \{i, j\}$, where $\mathbf{0}$ and $\mathbf{I}_3$ are, respectively, the null and identity matrices of order three, and n_n is the number of nodes of the whole structure.

3. Internal load vector for a membrane element

The Argyris' natural triangular membrane finite element ([4], [5], [6]) is defined in an *initial configuration*, in which it is already under a given stress field. Element nodes and edges are numbered anticlockwise, with edges facing nodes of same number. Nodal coordinates are referred to a global Cartesian system, and a local coordinate system, indicated by an upper hat, is adapted to every element configuration, such that the $\hat{x}$ axis is always aligned with edge 3, oriented from node *1* to node *2*, whilst the $\hat{z}$ axis is normal to the element plane.

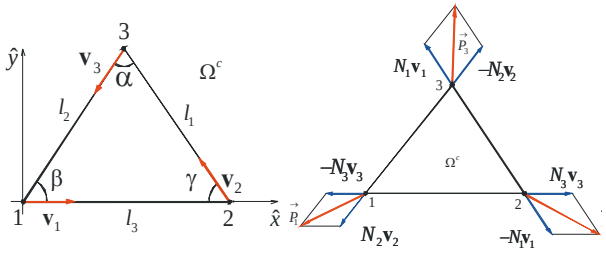

Figure 2: (a) Unit vectors $\mathbf{v}_i$, $i = 1,2,3$, along the element edges; (b) internal nodal forces $\mathbf{p}_i$, decomposed into natural forces $N_i\ \mathbf{v}_i$.

Current global coordinates of the element nodes, are given by $\mathbf{x}_i = \mathbf{x}_i^0 + \mathbf{u}_i$, $i = 1,2,3$, where $\mathbf{u}_i$ are the nodal displacements. The lengths of element edges are given by $\ell_i = \|\mathbf{l}_i\| = \|\mathbf{x}_k - \mathbf{x}_j\|$, with indexes $i, j, k = 1,2,3$ in cyclic permutation. Unit vectors parallel to the element edges are denoted by $\mathbf{v}_i = \mathbf{l}_i / \|\mathbf{l}_i\|$. With these definitions, the *vector of internal nodal forces* can be decomposed into forces parallel to the element edges, according to

$$\mathbf{p}^e = \begin{bmatrix} \mathbf{p}_1 \\ \mathbf{p}_2 \\ \mathbf{p}_3 \end{bmatrix} = \begin{bmatrix} N_2\mathbf{v}_2 - N_3\mathbf{v}_3 \\ N_3\mathbf{v}_3 - N_1\mathbf{v}_1 \\ N_1\mathbf{v}_1 - N_2\mathbf{v}_2 \end{bmatrix} = \begin{bmatrix} \mathbf{0} & \mathbf{v}_2 & -\mathbf{v}_3 \\ -\mathbf{v}_1 & \mathbf{0} & \mathbf{v}_3 \\ \mathbf{v}_1 & -\mathbf{v}_2 & \mathbf{0} \end{bmatrix} \begin{bmatrix} N_1 \\ N_2 \\ N_3 \end{bmatrix} = \mathbf{C}\mathbf{N} \tag{5}$$

where **C** is a geometric operator, which collects the unit vectors parallel to the element edges and $\mathbf{N} = \begin{bmatrix} N_1 & N_2 & N_3 \end{bmatrix}^T$ is the *vector of natural forces.*

If linear kinematic relationships hold, there exists also a linear relationship $\mathbf{N} = \mathbf{k}_n^r \mathbf{a} + \mathbf{N}_0$, where $\mathbf{a} = \begin{bmatrix} \Delta\ell_1 & \Delta\ell_2 & \Delta\ell_3 \end{bmatrix}^T$, is the *vector of natural displacements* (with $\Delta\ell_i = \ell_i - \ell_i^0$, $i = 1,2,3$) and the *element natural stiffness* is a constant matrix given by $\mathbf{k}_n^r = V_r \mathcal{L}_r^{-1} \mathbf{T}_r^{-T} \hat{\mathbf{D}} \mathbf{T}_r^{-1} \mathcal{L}_r^{-1}$, where V_r is the element volume, $\mathcal{L}_r = \text{diag}\left\{\ell_i^r\right\}$, $\hat{\mathbf{D}}$ collects the coefficients of Hooke's law for plane stresses, such that $\hat{\boldsymbol{\sigma}} = \hat{\mathbf{D}}\hat{\boldsymbol{\varepsilon}}$ and, finally, $\mathbf{T}_r$ is a transformation matrix, relating the linear Green strains $\hat{\boldsymbol{\varepsilon}}$ to the *natural strains* $\boldsymbol{\varepsilon}_n = \mathcal{L}_r^{-1}\mathbf{a}$, *i.e.*, $\boldsymbol{\varepsilon}_n = \mathbf{T}_r \hat{\boldsymbol{\varepsilon}}$, highlighting the fact that Argyris' natural membrane element is akin to a *strain gauge rosette* [6].

Since $\mathbf{k}_n^r$ has only six independent components, its storage is usually economic, reducing the number of operations required to calculate the internal loads, and thus the overall computing time. The vector of internal forces at each configuration is then given by

$$\mathbf{p}^e = \mathbf{C}\mathbf{k}_n^r \mathbf{a} \,. \tag{6}$$

The contribution of (6) to the global internal load vector is again given by (3), now with $\mathbf{A}_{1i}^e = \mathbf{A}_{2j}^e = \mathbf{A}_{3k}^e = \mathbf{I}_3$ and $\mathbf{A}_{1m}^e = \mathbf{A}_{2m}^e = \mathbf{A}_{3m}^e = \mathbf{O}$, $m \in \{1,2,\ldots,n_n\} \setminus \{i,j,k\}$.

3.1. A simple wrinkling model

Equation (6) holds for a linear-elastic isotropic material, working both in tension and compression. Since $\mathbf{k}_n^r$ is constant, it provides the fastest way to compute the internal nodal element loads, when the membrane is fully under tension. However, a membrane wrinkles instead of developing compressive stress. Thus, when wrinkling is detected, equation (6) has to be replaced for a lengthier calculation.

For linear isotropic materials, the principal stress and strain directions are parallel, and stress, strain or mixed wrinkling criteria are equivalent [7]. We choose a stress criterion and, instead of using (6), we first decompose the element natural stiffness into two different *3* x *3* constant matrices, according to

$$\mathbf{k}_n^r = \left(V_r \mathcal{L}_r^{-1} \mathbf{T}_r^{-T}\right)\left(\hat{\mathbf{D}} \mathbf{T}_r^{-1} \mathcal{L}_r^{-1}\right) = \mathbf{k}_\sigma^r \mathbf{k}_a^r \,. \tag{7}$$

In order to speed-up calculations, matrices $\mathbf{k}_\sigma^r = V_r \mathcal{L}_r^{-1} \mathbf{T}_r^{-T}$ and $\mathbf{k}_a^r = \hat{\mathbf{D}} \mathbf{T}_r^{-1} \mathcal{L}_r^{-1} = V_r^{-1} \hat{\mathbf{D}}\left(\mathbf{k}_\sigma^r\right)^T$ can be stored from the start. We then calculate element stresses according to

$$\hat{\boldsymbol{\sigma}} = \mathbf{k}_a^r \mathbf{a} + \hat{\boldsymbol{\sigma}}_0 \,, \tag{8}$$

and, after determining the principal stresses $\sigma_{1,2}$ and the "principal angle" θ_1 associated to $\hat{\boldsymbol{\sigma}}$, we modify stresses according to the following criterion:

$$\begin{cases} \sigma_1 \le 0 \;\; \Rightarrow \;\; \hat{\boldsymbol{\sigma}}' = \mathbf{0} \\ \sigma_2 \le 0 \;\; \Rightarrow \;\; \hat{\boldsymbol{\sigma}}' = \dfrac{\sigma_1}{2}\left[\left(1+\cos\theta_1\right) \;\; \left(1-\cos\theta_1\right) \;\; \sin\left(2\theta_1\right)\right]^T \\ \sigma_{1,2} > 0 \;\; \Rightarrow \;\; \hat{\boldsymbol{\sigma}}' = \hat{\boldsymbol{\sigma}} \end{cases} \tag{9}$$

Thereafter, we replace (6) by

$$\mathbf{p}^e = \mathbf{C}\mathbf{k}_\sigma^r \hat{\boldsymbol{\sigma}}' \tag{10}$$

4. Internal load vector for aufare's sliding-cable element

An *ideal* (or 'frictionless') *three-node sliding-cable element* (Figure 3), was initially considered by Aufaure [8]. Pauletti [9] generalized Aufare's element to include non-ideal sliding, and recast the formulation in a different notation. When non-ideal sliding is considered, the problem is no longer conservative. In the present work, however, only ideal sliding is considered.

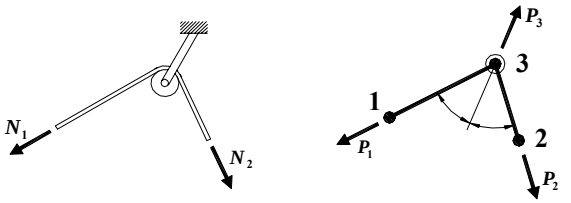

Figure 3: An Aufare's cable sliding without friction, or a cable passing through a pulley.

Keeping implicit the element index *e*, for basic quantities, the total length of the cable, in the current configuration, is given by the addition of the lengths of the two segments, $\ell = \left(\mathbf{l}_1^T\mathbf{l}_1\right)^{\frac{1}{2}} + \left(\mathbf{l}_2^T\mathbf{l}_2\right)^{\frac{1}{2}}$, where $\mathbf{l}_1 = \mathbf{x}_1^0 + \mathbf{u}_1 - \mathbf{x}_3^0 - \mathbf{u}_3$ and $\mathbf{l}_2 = \mathbf{x}_2^0 + \mathbf{u}_2 - \mathbf{x}_3^0 - \mathbf{u}_3$. The element is defined in an initial configuration, already subject to a normal force N_0. The initial length ℓ_0 is obtained from $\mathbf{l}_1^0 = \mathbf{x}_1^0 - \mathbf{x}_3^0$ and $\mathbf{l}_2^0 = \mathbf{x}_2^0 - \mathbf{x}_3^0$. The stress-free, reference length, considering linear-elastic behavior is given by $\ell_r = EA\ell_0 / \left(EA + N_0\right)$, and thus the normal load in the current configuration is $N = EA\left(\ell - \ell_r\right)/\ell_r$.

The Aufare's element internal forces vector is given by

$$\mathbf{p}^e = \begin{bmatrix} \mathbf{p}_1 \\ \mathbf{p}_2 \\ \mathbf{p}_3 \end{bmatrix} = \begin{bmatrix} \mathbf{v}_1 \\ \mathbf{v}_2 \\ -\left(\mathbf{v}_1 + \mathbf{v}_2\right) \end{bmatrix} N = \mathbf{C}N\,, \tag{11}$$

where the normal load N is uniform along the element, $\mathbf{v}_1$ e $\mathbf{v}_2$ are unit vectors supported by segments 1 and 2, and matrix $\mathbf{C}$ is a geometric operator. The contribution of (11) to the global internal load vector is again given by (3), now with $\mathbf{A}^e_{1i} = \mathbf{A}^e_{2j} = \mathbf{A}^e_{3k} = \mathbf{I}_3$ and $\mathbf{A}^e_{1m} = \mathbf{A}^e_{2m} = \mathbf{A}^e_{3m} = \mathbf{O}$, $m \in \{1,2,\ldots,n_n\} \setminus \{i,j,k\}$.

5. Internal load vector for a sliding-cable super-element

The *ideal (frictionless) sliding-cable super-element,* connects n_{se} nodes in a chain, as shown in Figure 4.

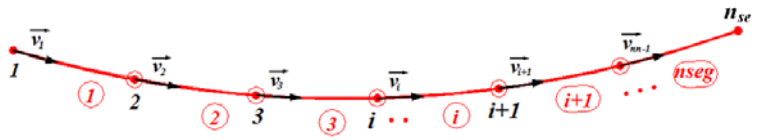

Figure 4: A super-element with n_{se} nodes sliding over n_{se}-2 pulleys. Numbers inside bullets refer to segments, numbers without bullets refer to nodes.

Associated to each segment $k = 1,\ldots,n_{se}-1$ we obtain a vector $\mathbf{l}_k = \mathbf{x}^0_{k+1} + \mathbf{u}_{k+1} - \mathbf{x}^0_k - \mathbf{u}_k$, and the total current cable length is given by $\ell = \sum_{k=1}^{n_{se}-1} \ell_k = \sum_{k=1}^{n_{se}-1} \|\mathbf{l}_k\|$. The element is defined in an initial configuration, already under a normal force N_0, uniform along the cable, since ideal, frictionless sliding is assumed. Defining $\mathbf{l}^0_k = \mathbf{x}^0_{k+1} - \mathbf{x}^0_k$, the cable length at the initial configuration is given by $\ell_0 = \sum_{k=1}^{n_{se}-1} \|\mathbf{l}_0\|$. Once again, for a linear-elastic material, the total reference (undeformed) cable length can be calculated by $\ell_r = EA\ell_0 / (EA + N_0)$, and the normal load at the current configuration is given by $N = EA(\ell - \ell_r)/\ell_r$.

The internal loads acting on the nodes $i = 1,\ldots,n_{se}$ of the super-element, at the current configuration, are given by $\mathbf{p}^{se}_i = N(\mathbf{v}_{i-1} - \mathbf{v}_i)$, where $\mathbf{v}_i = \mathbf{l}_i / \ell_i$. Further defining $\mathbf{v}_0 = \mathbf{v}_{n_{se}} = \mathbf{0}$, the vector of internal nodal loads of the sliding-cable super-element is given by

$$\mathbf{p}^{se} = \begin{bmatrix} \mathbf{p}_1 \\ \vdots \\ \mathbf{p}_i \\ \vdots \\ \mathbf{p}_{n_{se}} \end{bmatrix} = \begin{bmatrix} \mathbf{v}_0 - \mathbf{v}_1 \\ \vdots \\ \mathbf{v}_{i-1} - \mathbf{v}_i \\ \vdots \\ \mathbf{v}_{n_{se}-1} - \mathbf{v}_{n_{se}} \end{bmatrix} N = \mathbf{C}^{se} N, \qquad (12)$$

where $\mathbf{C}^{se}$ is a geometric operator, with the upper or lower indexes '*se*' added up to differentiate the sliding-cable super-element from a geodesic string, as discussed in the sequel. The contribution of (12) to the global internal load vector is again given by (3), now with $\mathbf{A}^{e}_{im} = \mathbf{I}_3$, if $m = 1, 2, \ldots n_n$ is equal the global node number of local node $i = 1, 2, \ldots n_{se}$, and $\mathbf{A}^{e}_{im} = \mathbf{O}$, otherwise.

6. Internal load vector for geodesic strings

It is a well known property that a cable sliding with no friction over a given surface will assume a geodesic configuration, with constant normal load acting along its full extension [10]. Thus a sequence of nodes, connected by truss elements of constant normal load, will rest along a geodesic line provided that, at each node, the component of the internal forces produced by these elements, normal to the membrane surface, is disregarded (otherwise the line would still accommodate to a (different) geodesic line, but the surface itself would be distorted). This sequence of nodes is called a *geodesic string* [11].

For both end-nodes of the geodesic string the internal load is kept zero, that is $\mathbf{p}^{gs}_1 = \mathbf{p}^{gs}_n = \mathbf{0}$, whilst for each intermediate node of the geodesic string, the inner load vector is modified according to

$$\mathbf{p}^{gs}_i = \mathbf{p}^{se}_i - \left(\mathbf{v}_i \mathbf{v}^T{}_i\right)\mathbf{p}^{se}_i = \left(\mathbf{I} - \mathbf{v}_i \mathbf{v}^T{}_i\right)\mathbf{p}^{se}_i = \mathbf{M}^{gs}_i \mathbf{p}^{se}_i , \tag{13}$$

where $\mathbf{M}^{gs}_i = \mathbf{I} - \mathbf{v}_i \mathbf{v}^T{}_i$, and $\mathbf{v}_i$ is the unit vector normal to the surface, at the i^{th} node. Therefore, defining $\mathbf{M}^{gs}_1 = \mathbf{M}^{gs}_{n_{gs}} = \mathbf{0}$, we have, for the whole geodesic-string, with *n* nodes:

$$\mathbf{p}^{gs} = \begin{bmatrix} \mathbf{M}^{gs}_1 & \mathbf{0} & \mathbf{0} & \mathbf{0} \\ \mathbf{0} & \mathbf{M}^{gs}_2 & \mathbf{0} & \mathbf{0} \\ \mathbf{0} & \mathbf{0} & \ddots & \mathbf{0} \\ \mathbf{0} & \mathbf{0} & \mathbf{0} & \mathbf{M}^{gs}_{n_{gs}} \end{bmatrix} \begin{bmatrix} \mathbf{p}^{se}_1 \\ \mathbf{p}^{se}_2 \\ \vdots \\ \mathbf{p}^{se}_{n_{gs}} \end{bmatrix} = \mathbf{M}^{gs} \mathbf{p}^{se} , \tag{14}$$

where $\mathbf{M}^{gs}$ is the "projection matrix" for the geodesic-string element.

It is seen that the internal load vector due to a geodesic string, equation (14), can be calculated in two steps: initially, an internal load vector $\mathbf{p}^{se}$, equivalent to a sliding-cable super-element is assembled; thereafter, at each node, the normal (to the surface) components is removed. Null operations in (14) are never performed. Finally, the contribution of (14) to the global internal load vector is again given by (3), now with $\mathbf{A}^{e}_{im} = \mathbf{I}_3$, if $m = 1, 2, \ldots n_n$ is equal to the global numbering of local node $i = 1, 2, \ldots n_{gs}$, and $\mathbf{A}^{e}_{im} = \mathbf{O}$, otherwise.

The normal vector $\mathbf{v}_i$ at a given node depends on the layout of all the facets converging to that node, and therefore the internal load vector associate to a geodesic-string cannot be computed without a loop over the adjacent membrane elements. Besides, since faceted

surfaces are not differentiable at edges and vertices, calculation of an "average normal vector" depends on some arbitrary definitions.

In Figure 5(a), symmetry requires $\mathbf{v}_i$ at apex of the pyramid to be parallel to the vertical axis. If each lateral face of the pyramid is represented by one triangular facet, a simple average of the normal vectors belonging to the four faces returns the correct normal at the apex node. However, if one face is divided into two areas, the simple average distorts the normal at the apex, as shown in figure 5(b). An area-weighted averaging again returns the correct normal as shown in figure 5(c), but if the face is further divided, even this criterion fails, as shown in Figure 5(d).

We have thus defined a new average nodal normal vector $\mathbf{v}_i$, according to

$$\mathbf{v}_i = \frac{\mathbf{w}_i}{\|\mathbf{w}_i\|} , \qquad \text{where } \mathbf{w}_i = \sum_{k=1}^{n_{ei}(i)} \mathbf{n}_k \theta_k , \tag{15}$$

and where $\mathbf{n}_k$, $k = 1,\ldots, n_{ei}(i)$ are the normal vectors of the surface elements incident to node *i*, whilst θ_k are the internal angles of that elements, at the incident vertices. It turns out that this angle-weighting provides an average normal vector which is invariant to the discretization, and returns a symmetric normal vector, as shown in figure 5(e).

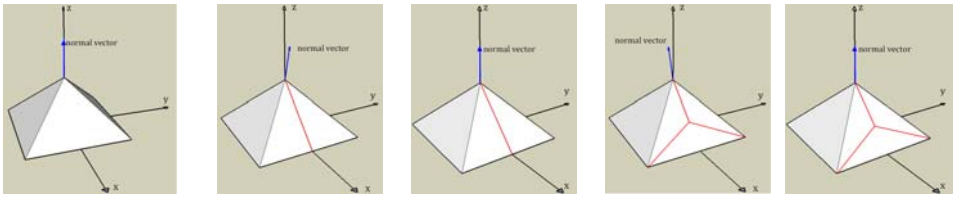

(a) simple average (b) simple average (c) area-weighted (d) area-weighted (e) angle-weighted

Figure 5: Average normal vectors at the apex of the same pyramid, due to different average criteria

7. Applications

Pauletti [2] applied the DRM to the processes of shape finding and patterning of the membrane roof of the "*Memorial dos Povos de Belém do Pará*" (MPBP), shown in Figure 6, using the actual design data to validate the implementation of the DRM into the program SATS – *A System for the Analysis of Taut Structures* [12]. An account on the design and construction of this 400m^2 membrane, located at the main city of the State of Pará, Brazil, is given in [13].

Figure 6: Membrane roof of the Memorial dos Povos of Belém do Pará.

In the present work, we investigate the response of a rough model of the MPBP membrane, under a uniform wind load $p = 286N/m^2$, acting upwardly over the whole membrane surface. All analyses were started from the same viable configuration (comprising geometry and stress field) determined in the phase of shape finding. The model had 120 nodes and 196 membrane elements, and the six vertices of the membrane were assumed to be fixed.

Results obtained with the SATS program, via dynamic relaxation, for both the "ideal-sliding" and the "fully-adherent" models were also compared with the results obtained for the same problem, still solve in SATS but via Newton iterations (as described in [1]. We have also used Ansys to solve the "fully-adherent" model and verify our wrinkling model, as also shown in [1].

Table 1 compares some selected results obtained with both the ideal-sliding and the fully-adherent models. All results presented very good agreement. Consideration of frictionless slippage led to an increase of only about 10% in maximum membrane displacements, but doubled the maximum first principal stresses (σ_I). Thus, results suggest that even if the global deformation of the membrane is little altered by the sliding conditions on the border cables, local stress concentrations can be considerably under-estimated, if sliding is disregarded. Of course, more numerical and experimental investigation is required before more definitive conclusions can be proposed, and that will be pursued in future works.

As a final example of application of the DRM, we consider the definition of some geodesic lines onto the membrane of the MPBP. The actual pattering used in MPBP, shown in Figure 8(a), was non-geodesic. A comparison with geodesic lines using a pure geometric algorithm was given in [14]. Figure 8(b) shows some geodesic lines obtained by means of the geometric procedure presented in that reference.

It was already pointed in [2] that when the geodesic line is distant from the initial string configuration, adjacent membrane elements may become quite distorted, due to large displacements of the string nodes. On the other hand, when the geodesic line is close to a line o element edges, the geometric procedure yields quite distorted elements, as can be seen in figure 8(b). Thus, geodesic strings can be quite convenient to adjust a mesh according to geodesic lines, shown in figure 8(c), which presents the geodesic lines obtained by means of geodesic strings.

Table 1. Comparison of selected results	Fully adherent model			Ideal sliding model	
	SATS- Newton	*SATS- Relax*	Ansys	SATS- Newton	*SATS- Relax*
Maximum Membrane Displacement [m]	0.40403	0.40343	0.40285	0.46468	0.46605
Maximum First Principal Stress σ_I [MPa]	13.60974	13.59338	13.6	26.49613	26.54674
Minimum Second Principal Stress σ_{II} [MPa]	0	0	0.000142	0	0
Maximum Second Principal Stress σ_{II} [MPa]	5.37598	5.37532	5.37	6.71951	6.73104

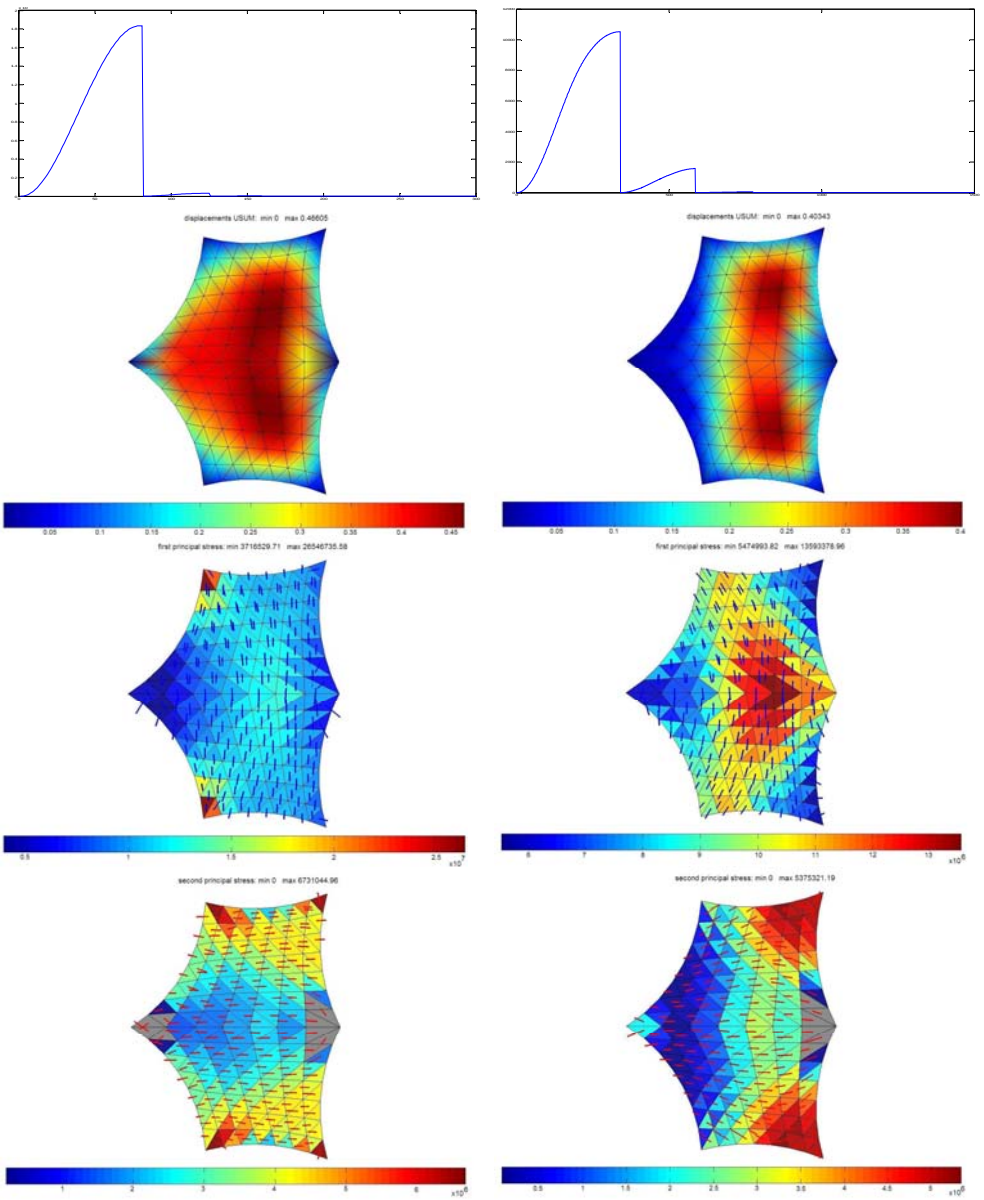

Figure 7: 1st column: ideal sliding model; 2nd column: fully adherent model.
1st row: kinetic energy transients; 2nd row: displacement norm fields; 3rd row: σ_I fields; 4th row: σ_{II} fields
(wrinkled elements shown in grey)

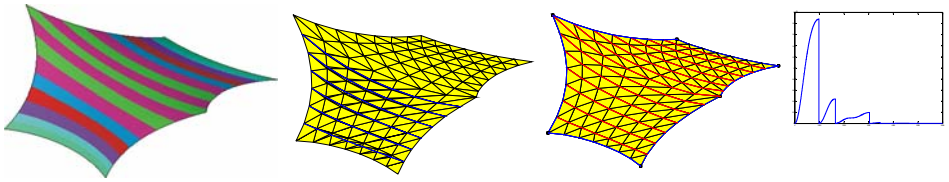

Figure 8: (a) MPBP non-geodesic patterns; (b) geodesic lines obtained via a geometric procedure (in blue) (c) geodesic lines obtained via a dynamic relaxation (in red); (d) kinetic energy transient.

Acknowledgement

The 1st author acknowledges the support by Nohmura Foundation for Membrane Structure´s Technology, Japan.

References

[1] Pauletti R.M.O. and Martins C.B., Modelling the slippage between membrane and border cables, *IASS Symposium*, Valencia, 2009.

[2] Pauletti R.M.O., Pappalardo A. Jr, Guirardi D.M., The method of dynamic relaxation for the static nonlinear analysis of cable and membrane structures. *IASS-SLTE International Symposium 2008*, Acapulco, Mexico.

[3] Barnes M.R., Form-finding and analysis of prestressed nets and membranes, *Computer & Structures* **30** (3), 685–695, 1988.

[4] Argyris J.H., Dunne P.C., Angelopoulos T., Bichat B., Large natural strains and some special difficulties due to non-linearity incompressibility in finite elements, *Comp. Meth. Appl. Mech.* Eng. **4** (2), 219–278, 1974.

[5] Pauletti R.M.O., Guirardi D.M., Deifeld T.E.C., "Argyris' Natural Membrane Finite Element Revisited". In E. Oñate e B. Kröpling (Eds.) *Textile Composites and Inflatable Structures*, CIMNE, Barcelona , 2005.

[6] Pauletti, R.M.O., Static Analysis of Taut Structures. In Oñate E, Kröpling B (Orgs.) *Textile Composites and Inflatable Structures II*, Springer-Verlag, 2008, 117-139.

[7] Miyazaki Y., Wrinkle/slack model and finite element dynamics of membrane, *Int. J. Numer. Meth. Engng* **66** 1179-1209, 2005.

[8] Aufaure M., A finite element of cable passing through a pulley, *Computer & Structures* **46** (5) 807–912, 1993.

[9] Pauletti R.M.O and Pimenta P.M., Formulação de Um Elemento Finito de Cabo Incorporando O Efeito do Atrito. *XV CILAMCE*, Belo Horizonte, 1994.

[10] Deregibus C. and Sassone M., Mathematical and Structural Properties of Geodesic Curves: An Application on a Free Form Gridshell, *IASS Journal* Vol. 49 n. 3 157-166, 2008.

[11] B.H.V. Topping and P. Iványi, *Computer Aided Design of Cable Membrane Structures*, Saxe-Coburg Publications, Kippen, Stirlingshire, Scotland, 2007.

[12] Guirardi D.M., Implementação de um elemento finito de membrana baseado na formulação natural de Argyris, MSc. Thesis (in Portuguese), *Polytechnic School, University of São Paulo*, 2006.

[13] Pauletti R.M.O. and Brasil R.M.L.R.F., Structural Analysis and Construction of the Membrane Roof of the 'Memorial dos Povos de Belém do Pará', *II Simposio Latinoamericano de Tensoestructuras*, Caracas, 2005.

[14] Dias U.S.Jr., Determinação dos padrões de corte em estruturas de membrana por linhas geodésicas. MSc. Thesis (in Portuguese). *Polytechnic School, USP*, 2006.